TISSUE ENGINEERING: Part A
Volume 20, Numbers 15 and 16, 2014

DOI: 10.1089/ten.tea.2013.0281

Nanoclay-Enriched Poly(ε-caprolactone) Electrospun Scaffolds for Osteogenic Differentiation of Human Mesenchymal Stem Cells

Akhilesh K. Gaharwar, PhD,[1–3,*,†] Shilpaa Mukundan, BTech,[3,4,†] Elif Karaca, MS,[3,4] Alireza Dolatshahi-Pirouz, PhD,[2–4] Alpesh Patel, PhD,[3,4] Kaushik Rangarajan, BTech,[3,4] Silvia M. Mihaila, MS,[3,4] Giorgio Iviglia, MS,[3,4] Hongbin Zhang, PhD,[3,4] and Ali Khademhosseini, PhD[2–6]

Musculoskeletal tissue engineering aims at repairing and regenerating damaged tissues using biological tissue substitutes. One approach to achieve this aim is to develop osteoconductive scaffolds that facilitate the formation of functional bone tissue. We have fabricated nanoclay-enriched electrospun poly(ε-caprolactone) (PCL) scaffolds for osteogenic differentiation of human mesenchymal stem cells (hMSCs). A range of electrospun scaffolds is fabricated by varying the nanoclay concentrations within the PCL scaffolds. The addition of nanoclay decreases fiber diameter and increases surface roughness of electrospun fibers. The enrichment of PCL scaffold with nanoclay promotes *in vitro* biomineralization when subjected to simulated body fluid (SBF), indicating bioactive characteristics of the hybrid scaffolds. The degradation rate of PCL increases due to the addition of nanoclay. In addition, a significant increase in crystallization temperature of PCL is also observed due to enhanced surface interactions between PCL and nanoclay. The effect of nanoclay on the mechanical properties of electrospun fibers is also evaluated. The feasibility of using nanoclay-enriched PCL scaffolds for tissue engineering applications is investigated *in vitro* using hMSCs. The nanoclay-enriched electrospun PCL scaffolds support hMSCs adhesion and proliferation. The addition of nanoclay significantly enhances osteogenic differentiation of hMSCs on the electrospun scaffolds as evident by an increase in alkaline phosphates activity of hMSCs and higher deposition of mineralized extracellular matrix compared to PCL scaffolds. Given its unique bioactive characteristics, nanoclay-enriched PCL fibrous scaffold may be used for musculoskeletal tissue engineering.

Introduction

Tissue engineering aims at repairing and regenerating biological tissues to improve the function of diseased or damaged tissue or organ.[1–5] As a direct result, there is an increase in the demand for developing new bioactive scaffolds that can facilitate the formation of functional tissue by directing stem cell differentiation.[6–9] Various processing techniques such as extrusion, solvent casting, porogen leaching, and electrospinning are investigated to fabricate different scaffold structures.[10,11] Among these techniques, electrospinning is extensively used to fabricate fibrous scaffolds, as it can mimic three-dimensional architecture of extracellular matrix (ECM).[1,10] The scaffolds architecture play a major role in controlling the human mesenchymal stem cells (hMSCs) differentiation, and, thus, electrospun scaffolds represents a promising approach for bone tissues engineering.[10]

During the past few decades, various polyesters have been investigated for tissue engineering applications due to their biocompatibility, bioresorbility, and high mechanical strength.[8,12–14] Among them, poly(ε-caprolactone) (PCL), a semi-crystalline and hydrophobic polymer with low glass transition temperature (−60°C) and moderate melting point (60°C), is an attractive polymer for musculoskeletal tissue engineering, as it can be used to fabricate a wide range of scaffold materials.[10,11] However, some of the problems associated with PCL include its slow *in vivo* degradation rate

[1]David H. Koch Institute for Integrative Cancer Research, Massachusetts Institute of Technology, Cambridge, Massachusetts.
[2]Wyss Institute for Biologically Inspired Engineering, Harvard University, Boston, Massachusetts.
[3]Center for Biomedical Engineering, Brigham and Women's Hospital, Harvard Medical School, Cambridge, Massachusetts.
[4]Harvard-MIT Division of Health Sciences and Technology, Massachusetts Institute of Technology, Cambridge, Massachusetts.
[5]Department of Maxillofacial Biomedical Engineering and Institute of Oral Biology, School of Dentistry, Kyung Hee University, Seoul, Republic of Korea.
[6]Department of Physics, King Abdulaziz University, Jeddah, Saudi Arabia.
*Current affiliation: Department of Biomedical Engineering, Texas A&M University, College Station, Texas.
†These authors contributed equally.

and lack of bioactive characteristics.[15] The degradation of PCL occurs due to hydrolytic cleavage of ester groups via the surface or bulk pathway.[11,16] Due to this degradation mechanism and hydrophobic nature, PCL takes more than 2 years to completely degrade *in vivo*.[15,16]

The degradation properties of PCL can be improved by incorporating nanoparticles such as hydroxyapatite, silica, magnetic nanoparticles, and synthetic clays within the polymeric scaffolds[11] or by blending PCL with other fast degrading polymers.[17] For example, Liao *et al.* incorporated hydroxyapatite nanoparticles within PLLA/PCL fibrous scaffolds to increase the biodegradation rate of the resulting constructs.[18] Electrospun scaffolds made from hydroxyapatite nanoparticles embedded in PCL had higher tensile strength and enhanced bioactivity while supporting osteoblast-like cell adhesion and proliferation.[19] The addition of silica (SiO_2) nanoparticles within electrospun PCL fibers also enhances the physical and chemical properties of the fibrous scaffolds.[20] Despite interesting physical, chemical, and biological properties, nanoparticle-reinforced PCL scaffolds lack osteogenic characteristics.

Nanoclays, also known as synthetic silicates, have shown to improve physical and mechanical properties of polymeric structures.[21,22] This is due to anisotropic and plate-like, high aspect-ratio morphology of nanoclay, which results in high surface interactions between the polymers and nanoparticles. Nanoclays are widely used to reinforce thermoplastic polymers in order to obtain hybrid composites with hierarchical structure,[23,24] elastomeric properties,[25] ultrastrong and stiff films,[26,27] super gas-barrier membrane,[28] superoleophobicity surfaces,[29] flame-retardant structures,[30] and self-healing hydrogels.[31] A recent study has shown that nanoclay (synthetic silicates nanoplatelets) can induce osteogenic differentiation in hMSCs without using any growth factors.[32] These unique bioactive properties of synthetic silicates may be processed to construct devices such as injectable tissue repair matrices, bioactive fillers, or therapeutic agents for triggering specific cellular responses toward bone-related tissue engineering approaches.

The addition of these synthetic silicates to polymeric matrix can be used to control physical and chemical properties of nanocomposite matrix.[33–35] Marras *et al.* fabricated PCL scaffolds enriched with organically modified nanoclay known as montmorillonite (MMT).[36] They observed that the incorporation of MMT with PCL matrix enhances mechanical strength without compromising ductility.[36] In a similar approach, the incorporation of halloysite nanoclay within electrospun PCL scaffolds increased the mechanical strength, protein adsorption, and cell adhesion of the resulting hybrid materials.[37] Despite interesting physical and chemical properties of clay-enriched nanocomposites, only a few studies have focused on using clay-based scaffolds for biomedical applications.[34,38,39] The addition of silicate nanoclay can be used to tune adhesion and spreading of fibroblast cells, preosteoblast cells, and hMSCs.[34,38] In another study, Ambre *et al.* showed that the addition of synthetic silicate to polymeric scaffolds consisting of chitosan and polygalacturonic acid promotes osteogenic differentiation of hMSCs.[40]

Here, we assessed the use of nanoclay-enriched electrospun PCL scaffolds for adhesion, proliferation, and differentiation of hMSCs. A range of nanoclay-enriched electrospun PCL scaffolds was obtained by changing the concentrations of nanoclay. The effects of nanoclay on surface morphology, degradation rate, thermal characteristics, mechanical properties, *in vitro* biomineralization, and cellular interactions were evaluated. We hypothesize that the nanoclay-enriched electrospun structure can support the osteogenic differentiation of hMSCs, along with the production of mineralized matrix. The features would enable the use of nanoclay-reinforced PCL scaffolds to design improved bioactive scaffolds for musculoskeletal tissue regeneration.

Materials and Methods

Fabrication of PCL–nanoclay electrospun scaffolds

PCL-$(C_6H_{10}O_2)_n$ with M_w ~70,000–90,000 Da was purchased (Sigma-Aldrich). Synthetic nanoclay (Nanofil®116) was obtained from Southern Clay Products, Inc. All other chemical and reagents are purchased from Sigma-Aldrich. The polymer solution was prepared by dissolving PCL (15% w/v) in 9:1 ratio of anhydrous chloroform and ethanol. We selected a 9:1 ratio of anhydrous chloroform and ethanol, as both PCL and nanoclay showed maximum solubility, compared to other solvents used for electrospinning. Then, nanoclay in different concentrations (0.1%, 1%, and 10% (w/w) with respect to PCL) was added to the solution. The electrospinning of PCL and nanoclay-enriched PCL was carried out using a 21G blunt needle at 12.5 kV (Glassman High Voltage) and a flow rate of 2 mL/h. The collector was a circular plate (diameter 6.5 cm) made of aluminum and maintained at a constant distance of 18 cm from the needle. These parameters were chosen based on our previous study on fabrication of PCL scaffolds.[41] The electrospun scaffolds were dried overnight in vacuum to remove the residual solvent.

Microstructure evaluation

The microstructure and morphology of electrospun fibers were evaluated by scanning electron microscopy (SEM) (JSM 5600LV; JEOL). The electrospun scaffolds were vacuum dried and then coated with gold/palladium (Au/Pd) for 2 min using a Hummer 6.2 sputter coater (Ladd Research). The images were captured using an accelerating voltage of 5 kV, a working distance of 5 mm, and a spot size of 20. The SEM images were analyzed using the Image J (NIH) software, and the fiber diameter was calculated from at least 100 fibers. The distribution of nanoclay within electrospun scaffold was determined by staining the nanoclay particles with food dye (red dye 40). The nanoclay stained with dye was separated from the solution by precipitating in organic solvents. Electrospun scaffolds were fabricated using red-stained nanoclay to determine the distribution of clay with the fibers. The optical images were obtained using Zeiss Axio Observer Z1 1 (AXIO1; Zeiss) that was equipped with Evolve EMCCD 512×512 16 μm pixels.

Accelerated in vitro *degradation*

Electrospun scaffolds were cut into 5 mm-diameter circular shapes and then subjected to accelerated degradation conditions ($n = 3$) by incubation in 5 mL of 0.5 mM sodium

hydroxide (NaOH) solution at 37°C. At various time points, the NaOH solution was carefully pipetted out, and the electrospun scaffold was washed 3× with distilled water. The samples were subsequently frozen using liquid nitrogen and then lyophilized. Then, the weight of the degraded sample (W_t) was measured, and the percentage mass loss for a given sample was calculated as $((W_o - W_t)/W_o \times 100)$, based on the initial mass (W_o) of the sample before incubation.

Chemical and thermal characterizations

The deposition of minerals (hydroxyapatite and/or calcium phosphate) on electrospun fiber after incubating in 10× SBF was evaluated using ALPHA Fourier Transform Infrared Spectroscopy (FTIR) Spectrometer (Bruker) in the wavenumber range of 4000–400 cm^{-1}. The thermal properties of electrospun scaffolds were investigated using a differential scanning calorimeter (DSC) (DSC 8500; Perkin-Elmer) and a thermogravimetric analyzer (Pyris 1 TGA; Perkin-Elmer). To prepare samples for DSC, the electrospun scaffolds were weighed (between 3–5 mg) in standard aluminum pans, sealed with lids, heated at the rate of 10°C/min from −70°C to 150°C, and then cooled from 150°C to −70°C using nitrogen as a purge gas. The second cycle (heating and cooling) was used to determine melting temperature (T_m), melting enthalpy (H_m), crystallization temperature (T_c), and crystallization enthalpy (H_c). The crystallinity (X_c) of the PCL in the electrospun fibers was calculated as $\Delta H_m/\Delta H_m^o \ (1/m_{PCL}) \times 100\%$, where ΔH_m^o is 136 J/g, which is the theoretical heat of fusion for 100% crystalline PCL,[42,43] and m_{PCL} is the mass fraction of PCL in the nanocomposite fibers ($m_{PCL} = 1$ for PCL fibers and $m_{PCL} = 0.9$ for PCL-10% Nanoclay). For TGA, samples were heated in a ceramic pan at the rate of 10°C/min from 50°C to 600°C under a constant stream of nitrogen at a flow rate of 20 mL/min.

Mechanical testing

The mechanical properties of electrospun scaffolds were investigated by performing uniaxial tensile tests using an Instron 5542 mechanical machine (Instron). Electrospun scaffolds (5 mm wide and 1 cm in length) were tested at a rate of 10 mm/min until fracture. The thickness of fibrous scaffolds was obtained between 100 and 200 μm. Mechanical properties such as elastic modulus (EM), ultimate strain, and fracture stress were calculated from the stress-strain curve. The EM was determined as the initial slope of the strain/stress curve, corresponding to 5–15% strain.

In vitro *biomineralization*

The ability of electrospun scaffold to facilitate biomineralization was evaluated using simulated body fluid (SBF). The electrospun scaffolds with different concentrations of nanoclay (0%, 0.1%, 1%, and 10%) were cut into 4×4 mm squares. The cut scaffolds were incubated with 2 mL of 10× SBF solution (prepared using a previously reported method)[44,45] at 37°C. After 2 h, the solution was removed and scaffolds were washed thrice with distilled water. The samples were frozen in liquid nitrogen and subsequently lyophilized for SEM imaging and FTIR.

Protein adsorption

Electrospun scaffolds ($n = 3$) that were 3 mm in diameter were washed thrice with phosphate-buffered saline (PBS). The samples were allowed to soak in 500 μL of 10% fetal bovine serum (FBS; Gibco) for 24 h at 37°C. The fibrous samples were washed thrice with PBS to remove any nonspecific adsorbed proteins. The samples were then treated with 2% SDS solution for 6 h in a shaker (50 rpm) to remove the adsorbed proteins. The supernatant was collected separately by centrifuging the samples, and the eluted proteins were analyzed using micro Bicinchoninic acid (BCA) protein assay reagent (Pierce BCA; Thermo Scientific) using the manufacturer's protocol.

Cell culture studies

Bone marrow-derived hMSCs (PT-2501; Lonza) were cultured in normal growth medium (α-MEM [Gibco], supplemented with 10% of heat-inactivated FBS [Gibco] and 1% penicillin/streptomycin [100U/100 μg/mL; Gibco]), at 37°C, in a humidified atmosphere with 5% CO_2. The cells were cultured until 70–75% confluence and were used before passage 5 for all the experiments. Before the trypsinization of cells (CC-3232; Lonza), the electrospun scaffolds were sterilized using ethanol for 30 s and added to well plates. Then, the cells were seeded on electrospun scaffolds ($1 \times 1\ cm^2$) at a density of 20,000 cells/scaffold in normal growth medium, in 24-well plates. After 24 h, the medium was replaced with the normal or osteoinductive media (500 μL/sample). Osteoinductive media consisted of normal growth medium that was supplemented with 10 mM β-glycerophosphate (Sigma Aldrich), 50 μg/mL ascorbic acid phosphate (Sigma Aldrich), and 10^{-8} M dexamethasone (Sigma Aldrich). The effect of nanoclays on cell proliferation was evaluated using Alamar Blue Assay (Invitrogen) on day 3 using standard protocol. The effect of nanoclays on the metabolic activity of hMSCs was evaluated using Alamar Blue Assay (Invitrogen) on day 1 and 7 using the manufacturer's protocol.

Actin cytoskeleton organization was observed using fluorescence microscopy. Cell-seeded scaffolds were fixed in 4% paraformaldehyde (PF) solution, and the cell membrane was permeabilized using 0.1% Triton X-100 for 30 min. Subsequently, the samples were blocked in 1% bovine serum albumin (BSA) and the actin cytoskeleton was stained using a 1:40 dilution of Alexa Fluor-594 phalloidin (Abcam) in 0.1% BSA. The cell nuclei were stained with 4′,6-diamidino-2-phenylindole (DAPI). The fluorescence images were obtained using Zeiss Axio Observer Z1 1 (AXIO1) that was equipped with a color camera (Evolve EMCCD 512×512 16 μm pixels).

Alkaline phosphatase (ALP) activity was measured using a colorimetric endpoint assay (ALP Colorimetric Assay Kit, ab83369), which quantified the conversion of *p*-nitrophenol phosphate (*p*NPP) to yellow *p*-nitrophenol by ALP enzyme. Briefly, at the determined time points, samples were retrieved and subjected to osmotic and thermal shocks to collect the cell lysate. The assay buffer solution of 5 mM *p*NPP and the samples (cell lysate) were added to a 96-well plate. After 1 h, the absorbance was read at 405 nm using a microplate reader (Epoch microplate reader; Biotek). A standard curve was made from standards (0–20 μM)

prepared with a *p*NPP solution. Sample and standard triplicates were analyzed, and sample concentrations were noted from the standard curve. The ALP activity was normalized with the DNA content. The amount of double-stranded DNA (dsDNA) was measured using a PicoGreen dsDNA Quantification Kit (P7589; Invitrogen) according to the manufacturer's protocol. The expression of ALP was also determined using Nitro-blue tetrazolium/indolylphosphate (NBT/BCIP) staining. First, the cells were washed with PBS, and then, 0.5 mL of NBT/BCIP was added to the samples. The samples were incubated at 37°C in a humidified chamber containing 5% CO_2 for 30 min. After that, the samples were washed with PBS and fixed with 4% PF. The imaging was performed using Zeiss Axio Observer Z1 1 (AXIO1) that was equipped with Evolve EMCCD 512×512 16 μm pixels.

The mineralized matrix produced by hMSCs was determined using Alizarin Red Staining. At 21 days, cells were fixed with 10% formalin (20 min) and then washed thrice with PBS. The fixed cells were further washed with distillated water in order to remove any salt residues and then, a solution of 2% (wt/v) Alizarin Red S (ARS; Sigma Aldrich) with a pH adjusted to 4.2, was added so that it covered the entire surface of the scaffolds. After 10 min of incubation at room temperature, the excess ARS was washed with distillated water. The ARS staining was imaged using a Zeiss Discovery V8 Stereo Microscope (DISV8).

Statistical analysis

Experimental data were presented as mean ± standard deviation ($n = 3$ to 5). Statistical differences between the groups were analyzed using one-way analysis of variance using Tukey *post-hoc* analysis. Statistical significance was represented as $*p < 0.05$, $**p < 0.01$, and $***p < 0.001$.

Results and Discussion

Effect of nanoclay on fiber morphology

The fibrous scaffolds of PCL and PCL-nanoclay composites were obtained by the electrospinning process as shown in Figure 1a. The effect of nanoclay on the surface morphology and fiber diameter of the electrospun scaffolds was investigated by using SEM. The results indicated that the scaffolds made of pure PCL showed uniform and smooth surface morphology of the electrospun fibers (Fig. 1b). These results were in accordance with the previously reported studies.[17,41] However, with the addition of nanoclay, the fiber diameter was decreased and the surface morphology of the fibers became rough. The fiber diameter was quantified using ImageJ, and it was observed that the average diameter of fibers for scaffolds made of pure PCL was around 5.6 ± 0.6 μm ($n = 100$) (Fig. 1c). The addition of 1% nanoclay reduced the average diameter of the electrospun fibers to 3.5 ± 0.5 μm. A further increase in the nanoclay concentration (10%) resulted in the formation of beaded structures embedded in the sub-micron fibrous structure (with an average diameter of 600 ± 50 nm). The decrease in the fiber diameter can be attributed to an increase in electron charge density of the prepolymer solution due to the addition of nanoclay. In addition, the nanoclay may have disrupted the molecular cohesion of the PCL chains in solution and resulted in the formation of beaded microstructures.

Apart from the decrease in the fiber diameter, surface roughness also depends on the nanoclay concentration. Pure PCL fibers were smooth at microscale, while the addition of nanoclay introduced surface roughness on the electrospun fibers. The effect was more prominent in the nanocomposite scaffolds containing 1% and 10% nanoclay, which showed higher surface roughness compared to PCL scaffold. A similar effect was shown earlier when nanohydroxyapatite (nHA) was incorporated in electrospun PCL.[46] In a similar study, the addition of nHA to collagen type I[47] or silk fibroin[48] also resulted in the formation of electrospun fibers with high surface roughness compared to the fibers containing only polymer. These studies also emphasized that surface roughness influences physical, chemical, and biological properties of electrospun scaffolds.[46–48] In the subsequent sections, we investigated the effect of nanoclay on the biodegradibility, thermal stability, mechanical strength, and bioactivity of the scaffolds.

Nanoclay promoted in vitro *degradation of fibrous scaffolds*

The degradation of PCL mainly occurs through hydrolytic cleavage of ester groups that can result from either surface or bulk degradation.[11,16] The degradation of PCL is a slow process and takes more than 2 years under *in vivo* conditions.[16] However, bone regeneration is a relatively fast process and takes 2 to 3 months to fully regenerate small bone defects. So, for bone tissue engineering, an ideal scaffold should have a faster degradation rate and should match the regeneration rate of damaged tissue. Thus, for PCL-based scaffolds, we would prefer to have a shorter degradation time. The degradation mechanism of electrospun PCL is different from its bulk degradation behavior due to the high surface to volume ratio. This is mainly due to the change in the hydrophobic characteristic and the higher crystallinity of PCL that are induced during the electrospinning process.[11] The degradation of electrospun PCL scaffold can be investigated by monitoring the weight loss of the scaffolds in accelerated degradation conditions.

The effect of nanoclay concentration on the degradation characteristic of electrospun fibers was investigated in accelerated conditions using 0.5 M NaOH solution (Fig. 2a). In our experiments, the electrospun PCL scaffolds took 112 h to completely degrade. The addition of nanoclay significantly reduces the time required for the complete degradation of electrospun scaffolds. For example, electrospun scaffolds containing 0.1% nanoclay were degraded in 108 h, whereas the scaffolds containing 1% and 10% nanoclay were degraded in 96 h respectively. The complete degradation was considered when the scaffold was dissociated into micro-fragments and the structural integrity was lost completely. The addition of the nanoclay promotes faster degradation of the PCL scaffolds. This may be due to the smaller fiber diameter and the lower hydrophobicity of PCL-nanoclay scaffolds compared to PCL scaffolds. The addition of nanoclay may facilitate the adsorption of water that renders PCL chains for hydrolytic degradation. Similar results were previously reported, indicating that the addition of tricalcium phosphate to PCL significantly accelerates the

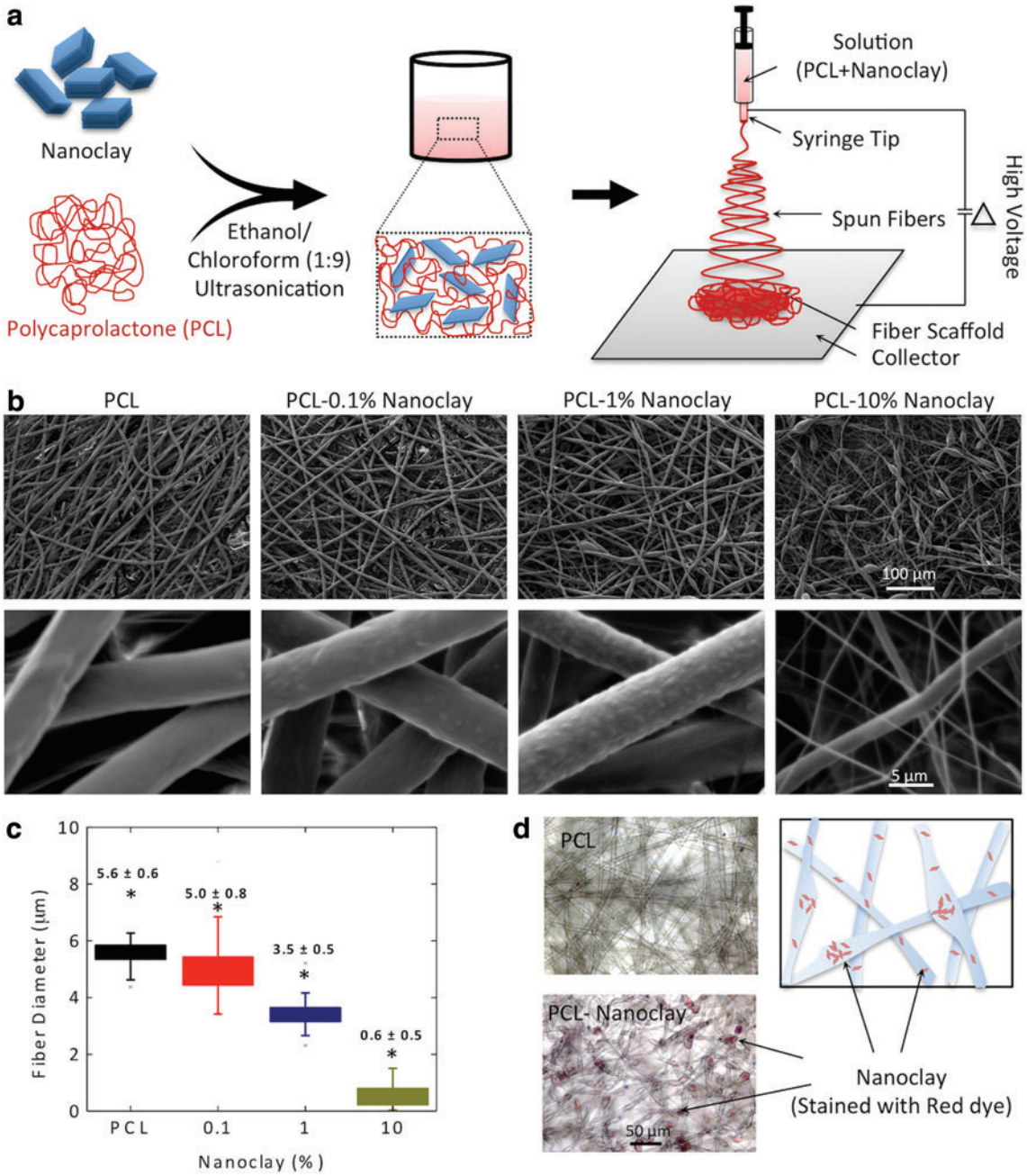

FIG. 1. Preparation of electrospun PCL-nanoclay nanocomposite fibers. **(a)** Schematic representation of the process to generate PCL/nanoclay composite fibers using electrospinning technique. The amount of nanoclay was varied from 0%, 0.1%, 1%, and 10% with regard to PCL. **(b)** The effect of nanoclay on fiber diameter and surface morphology of fibers. Pure PCL fibers show uniform size distribution and smooth surface morphology. The addition of silicate reduces fiber diameter and induces surface roughness. The effect appears to be prominent in electrospun fibers containing 1% and 10% nanoclay. **(c)** The effect of nanoclay on fiber diameter was quantified using image analysis. The average fiber diameter of PCL scaffolds is $5.6 \pm 0.6\,\mu m$. The addition of 1% and 10% nanoclay significantly reduced fiber diameter to 3.6 ± 0.5 and $0.6 \pm 0.5\,\mu m$. The data represent mean ± standard deviation ($n = 50$, ANOVA $^*p < 0.05$). The solid bars signify regions indicating 50% of the distribution of fiber diameter. **(d)** The distribution of nanoclay within the electrospun scaffold was determined by staining the nanoclay with a red dye. The scaffold containing nanoclay-formed beaded structures. ANOVA, analysis of variance; PCL, poly(ε-caprolactone). Color images available online at www.liebertpub.com/tea

degradation rate of the scaffolds due an increase in the diffusion of media within the scaffolds.[49]

To evaluate the effect of nanoclays on the degradation mechanism of the electrospun scaffolds, microstructural changes of electrospun fiber were investigated after subjecting the scaffolds to accelerated degradation conditions for 24 and 48 h (Fig. 2b). In pure PCL scaffolds, no significant structural damage was observed. However, we observed a decrease in fiber diameter after subjecting the PCL scaffold to the degradation medium for 48 h. This indicated

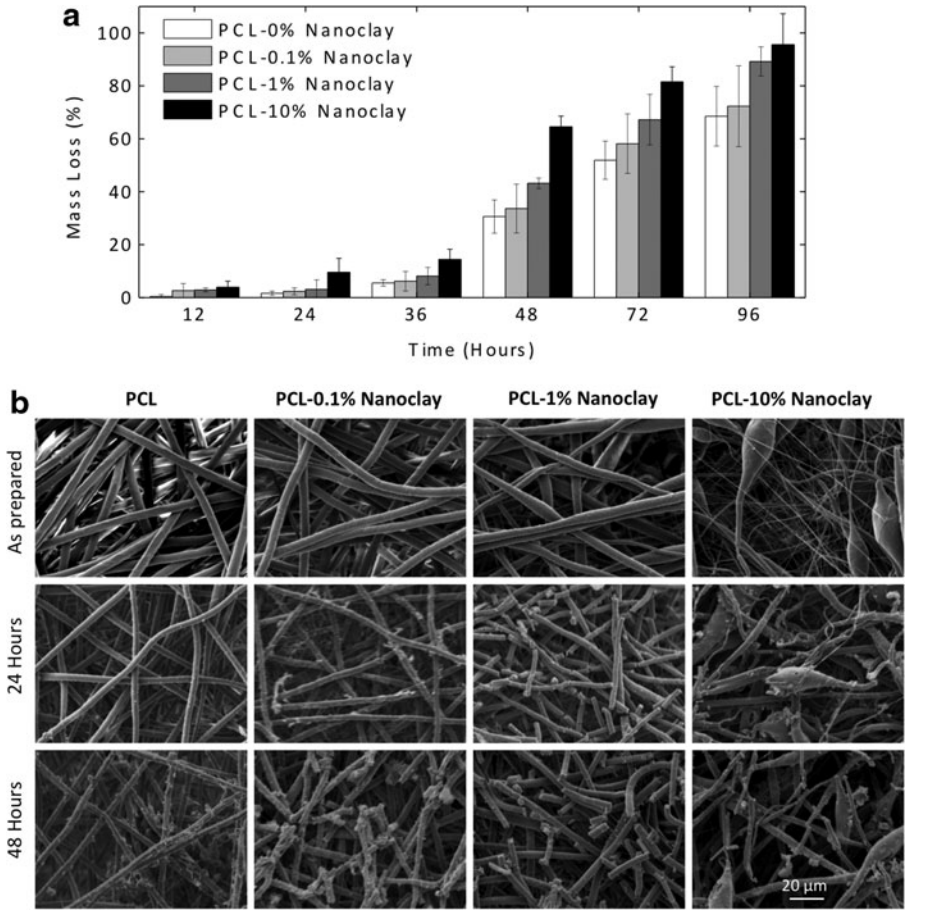

FIG. 2. The effect of nanoclay addition on the degradation of electrospun PCL scaffolds. **(a)** Electrospun PCL scaffolds degrade via surface degradation as depicted from the linear mass loss. The decrease in PCL fiber diameter was observed after 48 h in PCL scaffolds indicating surface degradation characteristic. The addition of nanoclay results in the bulk degradation of electrospun scaffolds. All the nanocomposite scaffolds show breakage of fibers in 24 and 48 h, respectively. In PCL-10% nanoclay fibers, smaller fibers quickly degraded, followed by bulk degradation of the thicker fibers. **(b)** The accelerated degradation of the electrospun scaffolds was determined by monitoring the weight loss of the fibrous structure over a period of 96 h. All the scaffolds showed a steady weight loss indicating gradual degradation of the scaffold. The scaffold containing 10% nanoclay showed enhanced degradation compared to PCL-only scaffolds indicating that nanoclay might promote the adsorption of water within the structure as well as the bulk degradation of PCL. The data represent mean ± standard deviation ($n = 5$).

that the degradation of electrospun PCL was dominated by surface erosion mechanism, similar to previously reported studies.[50] The addition of nanoclay indicated a distinct degradation behavior. For example, electrospun fibers containing 0.1% nanoclay showed fiber breakage after 48 h, whereas fibers containing 1% nanoclay showed significant structural degradation after 24 h. In electrospun scaffolds containing 10% nanoclay, thinner fibers were completely degraded within 24 h. The breakage of thicker fibers in nanoclay-enriched electrospun scaffolds indicated bulk degradation of the scaffolds. Overall, the addition of nanoclay to PCL significantly accelerates the degradation rate and facilitates bulk degradation behavior of the electrospun scaffolds.

Nanoclay-improved thermal stability of fibrous scaffolds

The effect of nanoclay on thermal characteristics of the electrospun scaffolds was investigated by DSC and TGA (Fig. 3). The DSC thermograms of heating and cooling cycles of electrospun PCL and nanoclay-enriched PCL scaffolds were shown in Figure 3a (the top panel is cooling curve, and the bottom panel is heating curve). PCL exhibited a peak melting temperature (T_m) of 57.26°C, and the melting enthalpy (ΔH_m) was calculated to be 47.99 J/g, which is similar to the trend observed in literature.[41] The electrospinning process significantly enhanced T_m and ΔH_m of electrospun PCL scaffold to 59.94°C and 66.95 J/g, respectively. This is mainly attributed to an increase in PCL crystallinity induced during the electrospinning process.

The addition of nanoclay to PCL did not result in a significant increase in T_m, but lowered ΔH_m by 4.81 J/g due to the addition of 10% nanoclay. This can be mainly attributed to a decrease in total PCL content in the electrospun scaffold. We further verified this by determining the effect of nanoclay on the degree of crystallization of polymer fraction in the electrospun fibers. The crystallinity of PCL beads was determined to be 35.28%. The electrospinning process resulted in an increase in polymer crystallinity to 49.22%, similar to the previously reported studies.[41] The crystallinity of PCL in the nanocomposite scaffold was determined to be around 49–50% (Fig. 3c), which was similar to the electrospun PCL scaffold. A slight increase in polymer crystallinity was observed due to the addition of nanoclay, indicating that the nanoclay particle may provide sites for crystallization.

The electrospun PCL scaffolds exhibited a crystallization temperature (T_c) of 28.79°C, similar to previous literature.[41] The addition of nanoclay significantly increases the crystallization temperature of electrospun scaffolds. For example, the addition of 0.1%, 1%, and 10% nanoclay results in crystallization temperatures of 29.75°C, 32.33°C, and 33.18°C, respectively. Similarly, the addition of nanoclay also results in a significant increase in the crystallization enthalpy (ΔH_c). The linear increase in T_c and ΔH_c suggests that the addition of nanoclay restricts chain mobility and facilitates heterogeneous nucleation of PCL within the scaffolds.

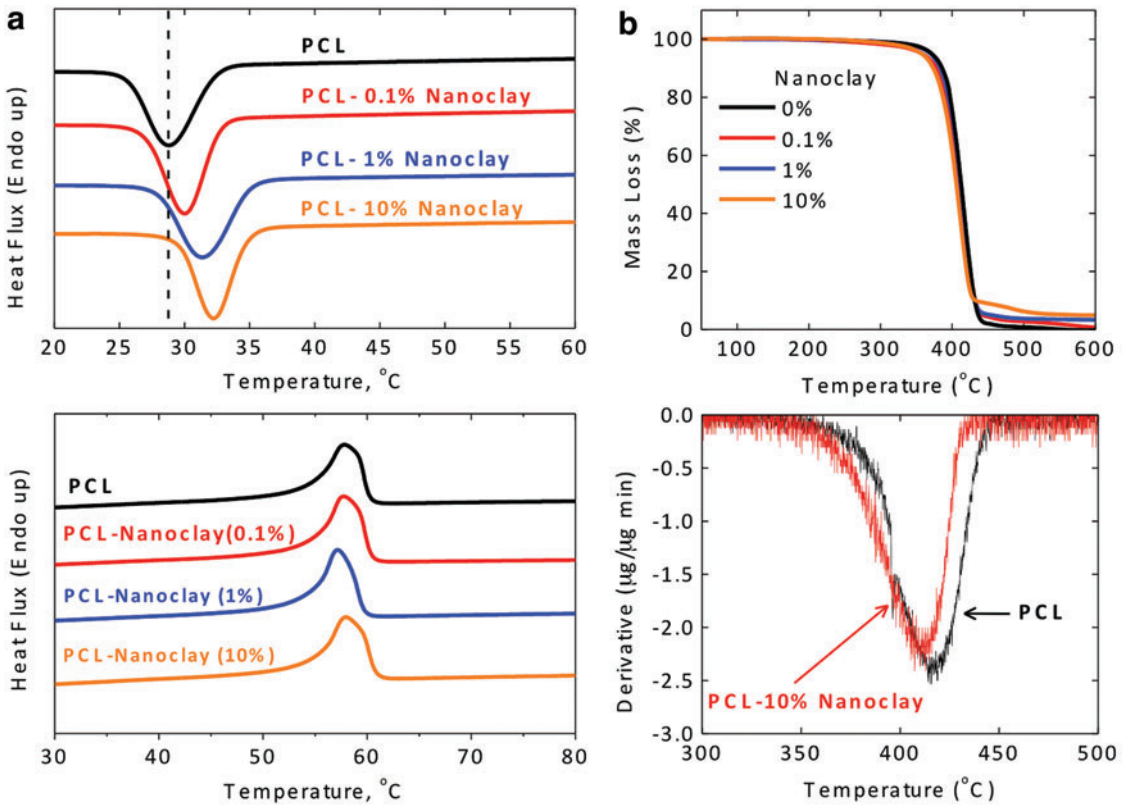

c

Samples	T_m(°C)	Delta H_m (J/g)	T_c(°C)	Delta H_c (J/g)	χ_c (%)	T_d(°C)
PCL Bead	57.26	47.99	24.40	-50.28	35.28	419.5
PCL Fibers	59.94	66.95	28.79	-50.97	49.22	416.8
PCL- 0.1% Nanoclay	59.40	66.95	29.75	-49.84	49.27	415.4
PCL- 1% Nanoclay	59.18	66.67	32.33	-48.72	49.51	412.2
PCL- 10% Nanoclay	59.63	62.14	33.18	-45.71	49.86	410.1

FIG. 3. Effect of nanoclay on thermal characterization of electrospun PCL fibers. **(a)** The differential scanning calorimeter thermograms showing cooling cycle (top panel), the addition of nanoclay-increased crystallization temperature (T_c), and the enthalpy of crystallization (delta H_c) indicate that nanoclay might be restricting polymer chain movements. The electrospinning of PCL results in an increase in polymer crystallinity (χ_c). The addition of nanoclay results in a slight increase in polymer crystallinity. Similarly, the heating cycles (bottom panel) of electrospun PCL and nanoclay-enriched PCL scaffolds indicate a significant increase in the melting temperature (T_m) and enthalpy of melting (delta H_m) when compared to PCL beads. The addition of nanoclay increased the thermal stability of nanocomposite due to an enhanced surface interaction between polymer and nanoclay. **(b)** TGA thermograph and DTGA profile indicate decreased thermal degradation temperature (T_d) due to the addition of nanoclay to PCL. **(c)** The summary of thermal properties of PCL and nanoclay-enriched PCL scaffolds. Color images available online at www.liebertpub.com/tea

Figures 3b shows TGA thermograms of electrospun PCL and nanoclay-enriched PCL scaffolds. Pure PCL scaffolds completely degrade within 440°C and negligible residue was observed, similar to that reported in the literature.[51] As expected, with an increase in nanoclay concentration, an increase in residual mass was observed. Similar results were observed by Marras *et al.*, due to the addition of organically modified MMT to electrospun polymeric scaffolds.[36] The TGA curve for electrospun PCL scaffold showed a single degradation profile with an inflection point around 420°C. The addition of 10% nanoclay decreased thermal degradation temperature of electrospun scaffold to 410°C. Moreover, the addition of nanoclay resulted in two distinct degradation slopes. The first slope corresponds to degradation of PCL, and the second slope corresponds to partial degradation of nanoclay. Derivative of TGA thermogram (DTGA) was determined to investigate the effect of nanoclay on degradation temperature. A significant shift in DTGA curve was observed due to the addition of nanoclay as observed in Figure 3b and c. Although we did not expect any covalent linkage between nanoclay and PCL, the shift in DTGA curve might be attributed to an enhanced surface interaction between PCL and nanoclay.

Effect of nanoclay on mechanical properties

Mechanical properties of scaffolds are important to evaluate their suitability for bone tissue engineering. The scaffolds for such application should be able to bear dynamic mechanical loading under *in vivo* conditions.[8]

Moreover, mechanical properties of scaffolds have a significant influence on hMSCs adhesion, proliferation, and differentiation.[52] The effect of nanoclay on mechanical properties of electrospun scaffolds was evaluated by a uniaxial tensile test (Fig. 4a, b). The electrospun PCL scaffolds had an EM of 4.8 ± 0.4 MPa, an elongation of $1050\% \pm 150\%$, and a fracture stress of 2.1 ± 0.3 MPa that is consistent with the literature.[17,41] The addition of a small amount of nanoclay (0.1%) resulted in a decrease in EM to 3.65 ± 0.8 MPa and an increase in elongation to $1160\% \pm 200\%$ and fracture stress to 2.8 ± 0.8 MPa. This indicates that the addition of a small amount of nanoclay results in more stretchable fibrous scaffolds. However, a further increase in nanoclay contents significantly reduced EM, ultimate strain, and fracture strain. This was mainly attributed to the decrease in fiber diameter due to the addition of nanoclay, as well as the discontinuities along the fibers also weakened the electrospun network. Moreover, nanoclays within the electrospun fiber might act as stress concentrators and result in lower mechanical performance.

The effect of nanoclays on the mechanical deformation was further investigated by determining fiber morphology of the electrospun fibers near the fractured region. In an electrospun PCL scaffold, uniform deformation was observed throughout the scaffold, which had a decrease in the fiber diameter as seen in Figure 4c. The addition of nanoclay significantly reduced the elastic deformation of electrospun scaffolds and resulted in the formation of small stress concentration regions. During the mechanical deformation, these small regions deform locally and lead to fracture. We have also evaluated the fiber morphology of the nanocomposite scaffolds (0.1%, 1%, and 10% nanoclay) at their extremities. At a lower nanoclay concentration, the fiber alignment was followed by the fiber deformation during the mechanical testing. However, at a higher nanoclay concentration, no significant mechanical deformation at the far end of the fractured edge was observed. We further evaluated fiber morphology at the fractured site, and found that the fracture mainly occurred due to pulling out of fibers and not due to uniform deformation of fibers. This was mainly attributed to the heterogeneous fiber size and the formation of beaded structures at higher nanoclay concentrations. For designing a scaffold for bone tissue engineering, the scaffolds should be able to withstand high mechanical strength. From the mechanical testing results, all the scaffolds have tensile modulus in the range of 1 to 5 MPa and elongation more than 100%. These properties are appropriate for deigning scaffolds for bone tissue engineering.[8] Moreover, these mechanical properties are also shown to have a favorable influence on the osteogenic differentiation of hMSCs.[52]

Nanoclay promoted in vitro *biomineralization*

A prerequisite for designing artificial materials for musculoskeletal tissue engineering is focused on developing bone-bonding materials. Previous studies have investigated these properties by subjecting artificial biomaterials (or scaffold) to SBF, an ionic mixture that resembles the body

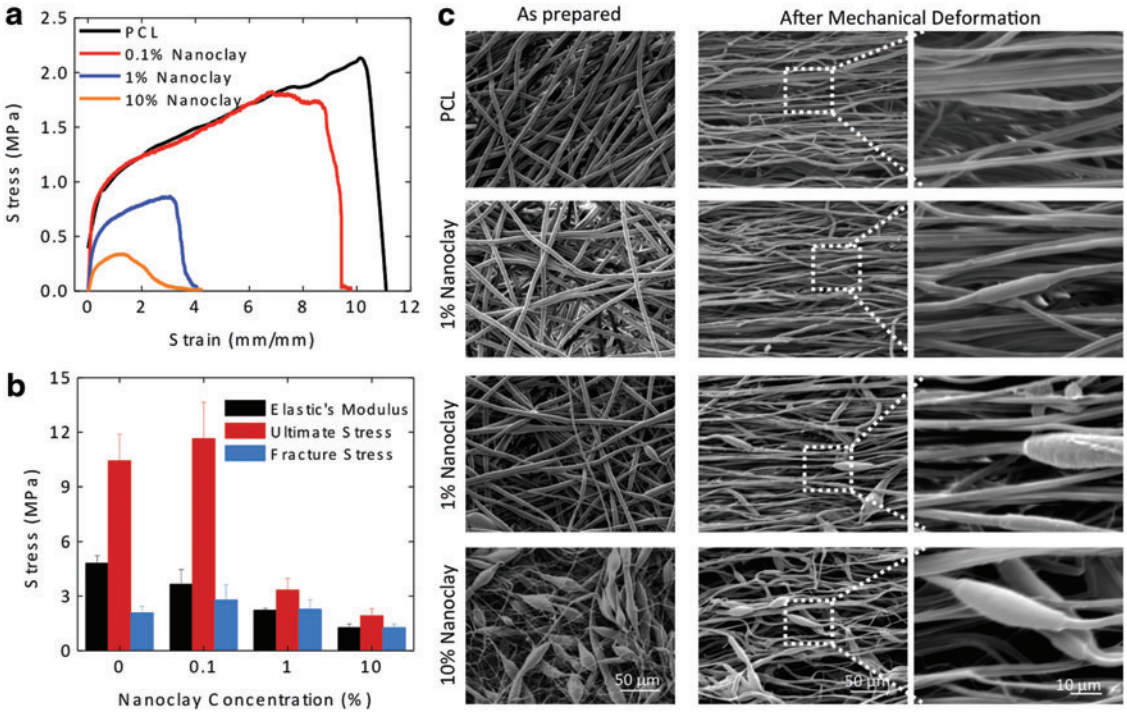

FIG. 4. Effect of nanoclay on the mechanical properties of electrospun PCL fibers. **(a)** Stress-strain curve of electrospun scaffolds subjected to uniaxial tensile stress was shown. **(b)** The addition of nanoclay significantly reduced elastic modulus, ultimate stress, and fracture stress. This is attributed to the decrease in fiber diameter due to the addition of nanoclay. The decrease in elongation was mainly attributed to the deformation of individual fibers. **(c)** The SEM images indicate that PCL scaffolds undergo uniform deformation when subjected to tensile stress. The addition of nanoclay resulted in a heterogeneous deformation and lower mechanical strength. SEM, scanning electron microscopy. Color images available online at www.liebertpub.com/tea

polyelectrolyte composition.[44,53] The *in vivo* bioactivity potential of these materials is highly correlated with the formation of apatite-like depots on the surface of the materials when exposed to SBF.[44,53] This method is an indirect indication of bone-bonding ability of newly designed biomaterials/scaffolds, as it can predict the formation of mineral structures that might lead to the integration of the scaffold with the bone.[44] The increase in the surface roughness of scaffolds aids in the biomineralization process by providing nucleation sites for mineral deposits when subjected to super saturated solution.[44] Bearing this in mind, the effect of nanoclays on the *in vitro* biomineralization of the electrospun scaffolds was assessed using SBF.

Figure 5a and 5b showed the effect of nanoclays on the biomineralization of electrospun PCL scaffolds. As expected, on pure PCL scaffolds, the deposition of minerals was observed, which correlates well with the previously reported studies.[54] PCL is a bioactive polymer and when exposed to physiological conditions, the surface of PCL fibers undergoes hydrolysis. This results in the formation of carboxylic (-COOH) group on the surfaces.[55] The negatively charged functional groups (-COOH) interact with calcium and phosphate ions present in SBF and facilitate the formation and deposition of hydroxyapatite crystals on the surface of the scaffolds.[55] The addition of nanoclays to electrospun scaffolds significantly enhances the amount of mineralized deposits as evident by the increase in the fiber diameter (Fig. 5a, b). At higher nanoclay concentrations, mineral deposits covering several fibers were observed, and at a 10% nanoclay concentration, it was difficult to identify individual fibers due to the presence of a continuous layer of mineral deposits.

We analyzed the mineral deposits using FTIR (Fig. 5c). Pure hydroxyapatite nanoparticles (positive control) are

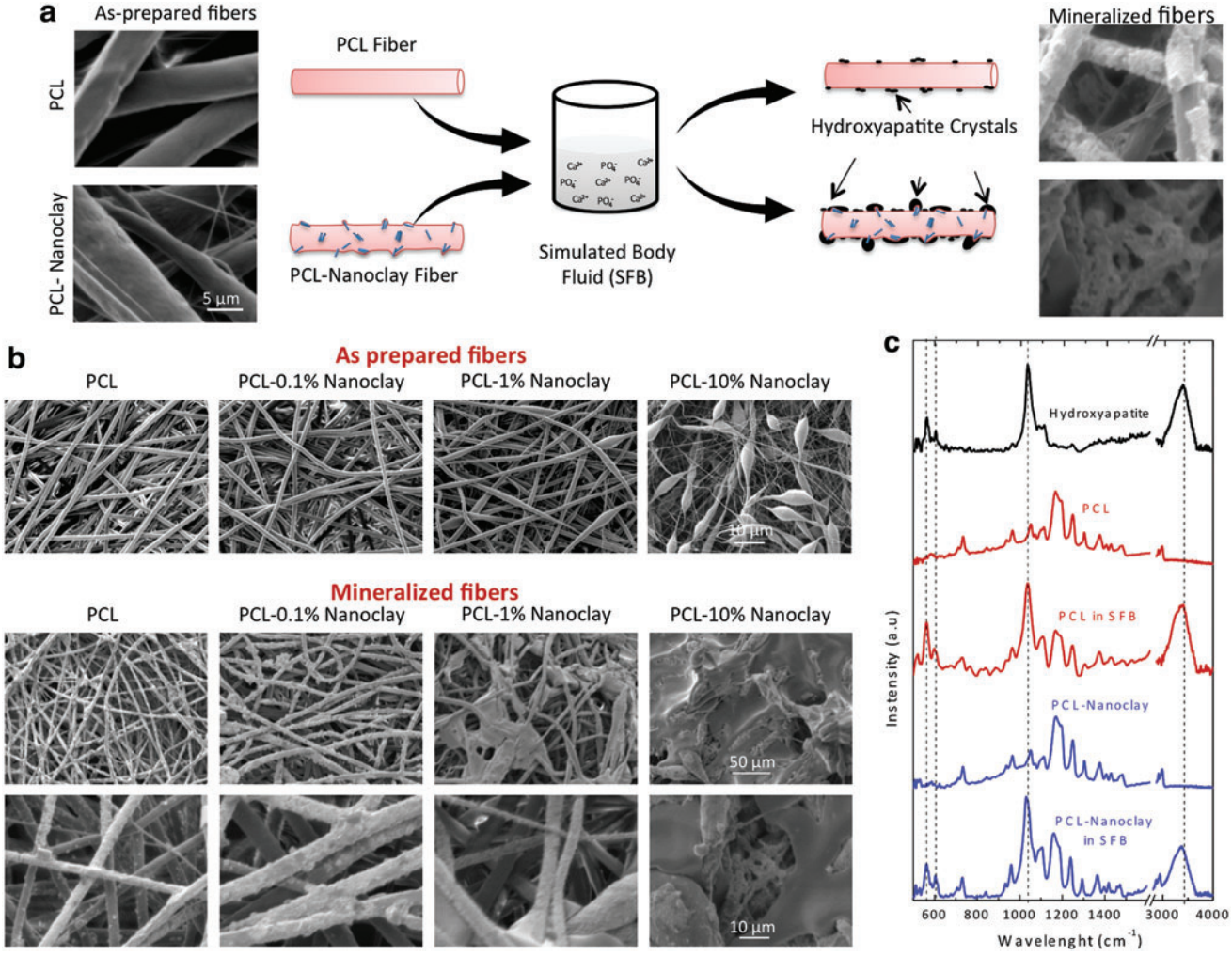

FIG. 5. Nanoclay promotes *in vitro* biomineralization on electrospun scaffold in simulated body fluid (SBF). **(a)** Since the prepared PCL scaffolds had uniform and smooth surface morphology, however after subjecting these electrospun scaffolds to 10× SBF for 2 h, the formation of mineralized layer on the fibers was observed. SBF is a super saturated solution of calcium and phosphate, and a bioactive surface when submersed in SBF promotes the formation of mineralized structure. **(b)** The SEM images indicated fiber morphology of the electrospun scaffolds before and after subjecting the scaffold to SBF. The addition of nanoclay to PCL significantly improved the biomineralization ability due to enhanced surface roughness. **(c)** The chemical nature of the deposited mineralized matrix was evaluated using FTIR. Hydroxyapatite has a strong peak at 1045 cm^{-1} that corresponds to the P-O stretching band. Both PCL and PCL-Nanoclay composites showed the formation of hydroxyapatite when submersed in SBF. FTIR, Fourier Transform Infrared Spectroscopy. Color images available online at www.liebertpub.com/tea

characterized by peaks at 1036, 603, and 567 cm^{-1}, corresponding to phosphate groups (PO_4^{3-}). We observed that after the treatment with SBF, both PCL and PCL-nanoclay fibers show strong phosphate peaks. However, the PCL-nanoclay scaffolds exhibit uniform coverage of the mineralized layer over the scaffold surface. In addition, due to inorganic nature of the nanoclays, a local microenvironment of concentrated inorganic polyelectrolyte is created, leading to the precipitation/deposition of the mineralized layer. Furthermore, the irregular fibrillar structure of PCL-nanoclay scaffolds provides the base for the formation of nucleation sites, essential for the growth of inorganic depots, which, in fact, is the prerequisite for fracture-healing processes.

Adhesion and proliferation of hMSCs on nanoclay-enriched PCL scaffolds

The multipotent nature and self-renewal ability of hMSCs make them the most clinically relevant cells to address the healing and reconstruction of tissues or organs.[52,56] In a native microenvironment, the cellular fate of these hMSCs is strongly dependent on the interaction with the surrounding cells, as well as with the ECM in which they are embedded.[57] *In vitro* strategies, aimed at mimicking these conditions, have employed the seeding or encapsulation of hMSCs on/in scaffolds aiming at their adhesion and proliferation, along with the triggering of their differentiation toward the desired lineage.[2,4,58] The initial response of hMSCs when seeded on a fibrous scaffold plays an important role in defining the subsequent biological events and their desired functionality. hMSCs rely on the adhesion on substrates that enable the organization of their cytoskeleton and sustain their proliferation, further dictating their behavior.[35,59]

The interaction of hMSCs with the scaffolds was evaluated by investigating their adherence and metabolic activity. The cells were able to adhere to the electrospun scaffolds, as they readily elongated their cytoskeleton along the fiber axis (Fig. 6a). However, no significant influence of nanoclay was observed on cellular adhesion. The effect of silicate on the metabolic activity of adhered cells was evaluated using Alamar blue assay. The metabolic activity of cells can be used as an indicator for cellular proliferation. The result indicates that cells seeded on the nanoclay-enriched PCL scaffolds exhibited significantly higher metabolic activity when compared to PCL scaffolds (Fig. 6b).

The adhesion and proliferation of hMSCs are dependent on the presence of cell-adhesive proteins as well as on the surface roughness of electrospun scaffolds. The addition of nanoclay did not significantly influences protein adsorption on the electrospun scaffolds. After 24 h, the amounts of protein adsorbed on the surface of PCL, PCL-0.1% Nanoclay, PCL-1% Nanoclay, and PCL-10% Nanoclay were 2.7 ± 0.2, 3.1 ± 0.5, 2.5 ± 0.3, 2.4 ± 0.2 μg/mL, respectively. This indicated that the adsorption of protein on the fibrous scaffold was not the major factor, and, thus, surface roughness may have been contributing to the increase in the metabolic activity of hMSCs. The roughness of these scaffolds (Fig. 1b), generated by the heterogeneous distribution of fiber diameter and nanoclays within the fiber, the cells can easily populate the substrate by anchoring and stretching

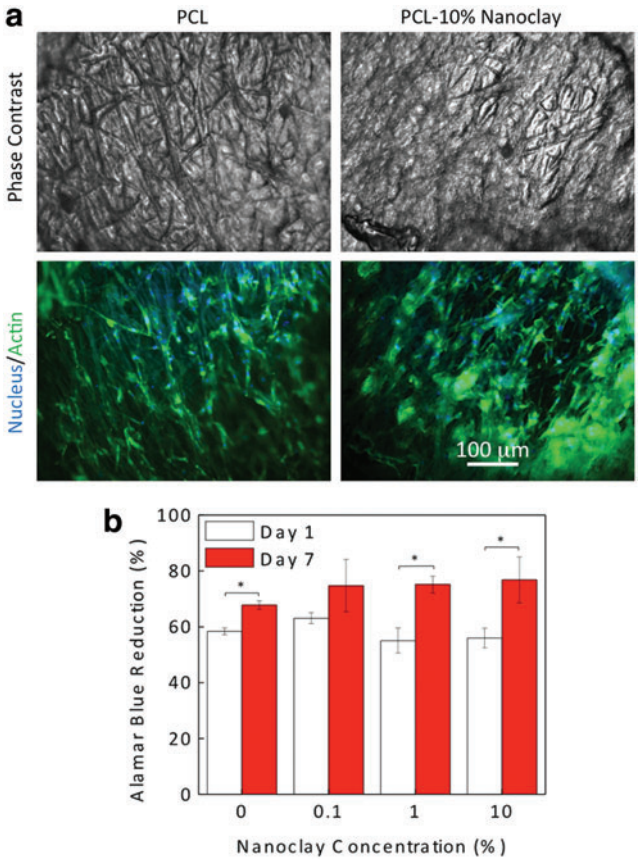

FIG. 6. Adhesion and proliferation of hMSCs on PCL and PCL-nanoclay electrospun scaffolds. **(a)** hMSCs readily attached and spread on the fibrous structure, and the cell bodies were stretched along the fiber axis (Day 3). However, no significant difference in cell attachment was observed due to the addition of nanoclay. **(b)** The proliferation of hMSCs was monitored using Alamar Blue on day 1 and 7 in normal media. hMSCs readily proliferate on PCL and nanoclay-enriched PCL scaffolds. However, no significant effect of nanoclay on cell proliferation was observed. The data represent mean ± standard deviation ($n = 3$, ANOVA $^*p < 0.05$). hMSCs, human mesenchymal stem cells. Color images available online at www.liebertpub.com/tea

their fillapodia on the micro-sized rough structure, leading to an increase in the metabolic activity of adhered cells. Earlier studies have also indicated a positive effect of nanoclay[39] and nanoparticles[60,61] on enhanced cell adhesion and proliferation.

Nanoclay enhanced ALP activity and promoted production of mineralized matrix

The effect of nanoclay on the osteogenic differentiation of hMSCs was investigated by seeding hMSCs on PCL and PCL-nanoclay scaffolds. The osteogenic differentiation of seeded hMSCs was monitored by determining ALP activity over a period of 21 days. The ALP is an early marker for the osteogenic differentiation of hMSCs, and its temporal pattern consists of an increase in its activity in the first time points, followed by a dramatic decrease, accompanied by the mineralization of the deposited ECM. We first evaluated the distribution of ALP on the substrate, and found that its

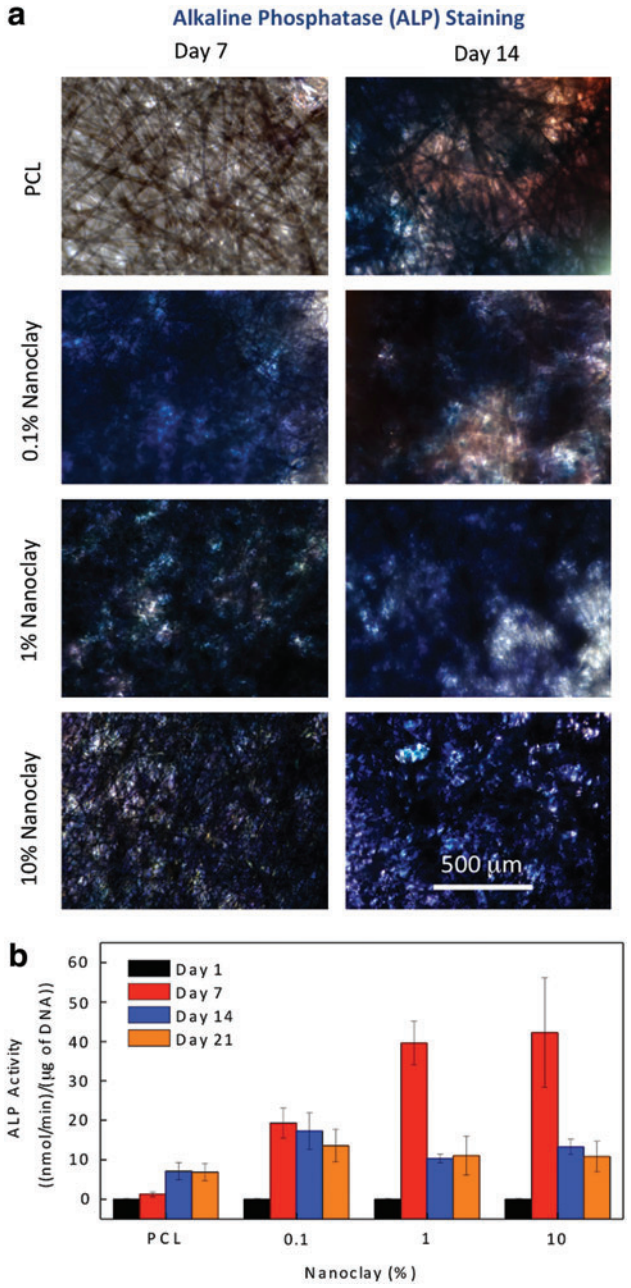

FIG. 7. Effect of nanoclay on osteogenic differentiation of hMSCs. **(a)** hMSCs were stained for surface alkaline phosphatase (ALP)-positive cells after 7 and 14 days. A uniform distribution of the ALP-positive cells on the scaffold can be observed, suggesting that the differentiation occurs in a homogeneous manner throughout the scaffolds. This is in correlation with the ALP activity result, where peak ALP activity in PCL scaffolds was observed on day 14 and in nanoclay-enriched PCL scaffolds, it was observed on day 7. **(b)** ALP activity of hMSCs seeded on electrospun scaffold was monitored over the period of 21 days. The ALP activity first increases and then decreases, presents a bell shape pattern, compatible with osteogenic differentiation of hMSCs. Briefly, no significant effect of nanoclay was observed on days 3, 14, and 21. However, on day 7, the nanoclay-enriched scaffolds showed significantly higher ALP activity compared to the PCL scaffolds. This indicates that the nanoclay from polymeric scaffold triggers and sustains the osteogenic differentiation of stem cells. Color images available online at www.liebertpub.com/tea

distribution was uniform on the entire surface of the scaffolds. However, the PCL scaffolds alone showed faded staining on day 7, when compared with (horizontal bars represent significant differences between groups, $*p < 0.05$, ANOVA) the nanoclay-enriched PCL that exhibited an intense purple coloration (Fig. 7a). However, by day 14, the ALP can be easily detected on the PCL scaffolds as well. Furthermore, the quantification of the ALP activity highlighted the presence of an intense peak at day 7, for the nanoclay containing scaffolds, while a delayed and moderate activity was detected for the PCL scaffolds only (Fig. 7b). The results indicate a strong correlation between ALP production and ALP activity.

The increase in the ALP activity sets the basis for a consequent intense bone-like proteins deposition, which will further act as a template for the mineralization. Thus, we evaluated the deposition of inorganic calcium, the hallmark of complete stabilization and maturation of the differentiated cells, to determine the extent of mineralization on each

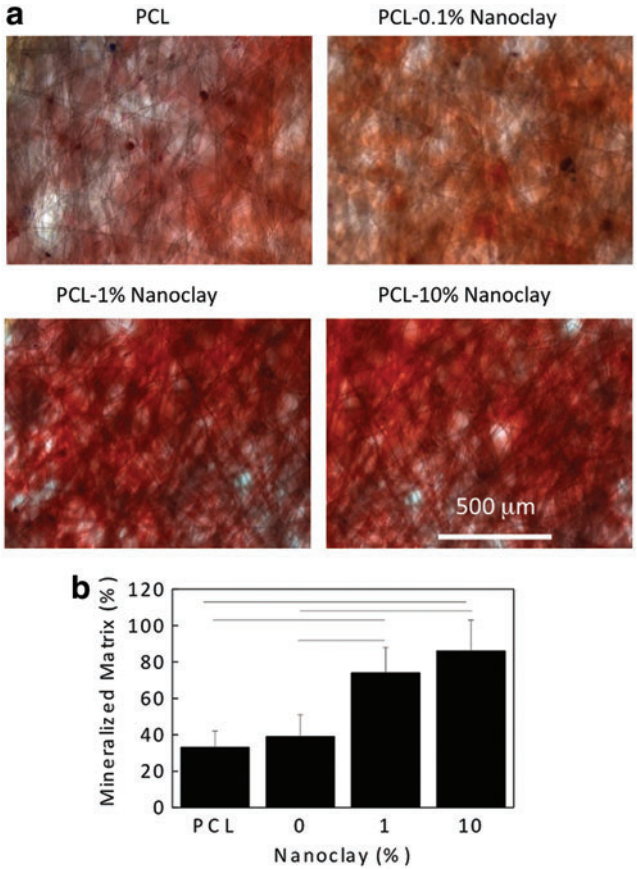

FIG. 8. Effect of nanoclay on the formation of mineralized matrix. **(a)** The production of mineralized matrix was evaluated using Alizarin Red S staining on day 21. The results indicate a significantly higher production of mineralized extracellular matrix in PCL-nanoclay composites compared to PCL scaffolds. This indicates that the nanoclay from polymeric scaffold triggers and sustains the osteogenic differentiation of stem cells. **(b)** The image quantification indicates the production of enhanced mineralized matrix coverage due to the addition of nanoclay. The bars represent mean ± standard deviation ($n = 3$; horizontal bars represent significant differences between groups, $p < 0.05$, ANOVA). Color images available online at www.liebertpub.com/tea

of the considered formulations. Since Alizarin Red specifically stains for inorganic calcium, it was possible to assess the distribution of the mineralized matrix on the PCL-based scaffolds (Fig. 8a). The red staining was found in all of the formulations; however, the nanoclay-enriched scaffolds displayed an intense-dark red coloration, suggesting that with the addition of the nanoclay to the PCL, hMSCs undergo an enhanced osteogenic differentiation. We further quantified the amount of mineralized matrix by analyzing the area of the stained region (Fig. 8b). The results correlated well with the ALP activity of hMSCs, and the scaffold containing 10% nanoclay showed the highest area fraction of stained region compared to all other scaffolds, whereas scaffolds containing 0.1% nanoclay have mineralized area fractions similar to the positive control. Earlier studies have shown that electrospun PCL support the osteogenic differentiation of hMSCs.[62] They observed that nanofibrous PCL scaffold supports the formation of mineralized matrix as compared to micron-size fibers. In a similar study, the incorporation of bioactive nanoparticles such as silica (SiO_2) to electrospun PCL was shown to induce and support osteogenic differentiation of hMSCs.[20] They observed that the addition of silica enhanced ALP activity and up-regulated the production of osteo-related extracellular proteins.[20]

Taken together, our results suggest that the addition of nanoclay to PCL scaffolds sustained and enhanced the osteogenic differentiation of seeded hMSCs, when compared to only the PCL. The increase in the hMSCs proliferation rate, followed by the burst in the ALP activity and the subsequent mineralization, are features that are of major importance when aiming at the designing of bioactive matrix for musculoskeletal tissue engineering.

Conclusion

We report on the fabrication and characterization of nanoclay-enriched electrospun PCL scaffold for controlling the differentiation of hMSCs. A range of electrospun scaffolds was fabricated by varying the nanoclay concentrations within the PCL scaffolds. The addition of nanoclay decreases fiber diameter and increases surface roughness of electrospun fibers. The enrichment of a PCL scaffold with nanoclay promoted *in vitro* biomineralization when subjected to SBF, indicating bioactive characteristics of the hybrid scaffolds. The slow degradation rate of PCL was improved due to the addition of nanoclay. The effect of nanoclay on the mechanical and thermal properties of electrospun fibers was evaluated. The feasibility of using nanoclay-enriched PCL scaffolds for tissue engineering applications was investigated using hMSCs. The addition of nanoclay significantly enhances the attachment, proliferation, and differentiation of hMSCs on the electrospun scaffolds. Furthermore, the nanoclay-enriched PCL scaffolds promotes ALP activity and the production of mineralized matrix, features that are attractive for refining and improving the bone tissue engineering outcomes.

Acknowledgments

A.K.G. would like to thank Robert S. Langer (MIT) for access to instruments and acknowledges financial support from MIT-Portugal Program (MPP-09Call-Langer-47). A.P. would like to acknowledge a postdoctoral fellowship (Fellowship No. PDF-388346-2010) awarded by the Natural Science and Engineering Research Council, Canada. H.Z. would like to acknowledge the National Natural Science Fund for Distinguished Young Scholars (Grant No. 51025313). This research was funded by the NIH (HL092836, EB021597, AR057837, and HL099073), the Deanship of Scientific Research (DSR), King Abdulaziz University (18-130-1434-HiCi), the Office of Naval Research Young Investigator award, and the Presidential Early Career Award for Scientists and Engineers (PECASE) CAREER award (AK).

Disclosure Statement

No competing financial interests exist.

References

1. Khademhosseini, A., Vacanti, J., and Langer, R. Progress in tissue engineering. Sci Am Mag **300,** 64, 2009.
2. Peppas, N.A., Hilt, J.Z., Khademhosseini, A., and Langer, R. Hydrogels in biology and medicine: from molecular principles to bionanotechnology. Adv Mater **18,** 1345, 2006.
3. Yang, S., Leong, K.-F., Du, Z., and Chua, C.-K. The design of scaffolds for use in tissue engineering. Part I. Traditional factors. Tissue Eng **7,** 679, 2001.
4. Khademhosseini, A., Langer, R., Borenstein, J., and Vacanti, J.P. Microscale technologies for tissue engineering and biology. Proc Natl Acad Sci U S A **103,** 2480, 2006.
5. Detamore, M.S., and Athanasiou, K.A. Motivation, characterization, and strategy for tissue engineering the temporomandibular joint disc. Tissue Eng **9,** 1065, 2003.
6. Hench, L.L., and Polak, J.M. Third-generation biomedical materials. Science **295,** 1014, 2002.
7. Nikkhah, M., Edalat, F., Manoucheri, S., and Khademhosseini, A. Engineering microscale topographies to control the cell-substrate interface. Biomaterials **33,** 5230, 2012.
8. Hutmacher, D.W. Scaffolds in tissue engineering bone and cartilage. Biomaterials **21,** 2529, 2000.
9. Benhardt, H.A., and Cosgriff-Hernandez, E.M. The role of mechanical loading in ligament tissue engineering. Tissue Eng Part B Rev **15,** 467, 2009.
10. Jang, J.H., Castano, O., and Kim, H.W. Electrospun materials as potential platforms for bone tissue engineering. Adv Drug Deliv Rev **61,** 1065, 2009.
11. Cipitria, A., Skelton, A., Dargaville, T.R., Dalton, P.D., and Hutmacher, D.W. Design, fabrication and characterization of PCL electrospun scaffolds-a review. J Mater Chem **21,** 9419, 2011.
12. Patel, A., Gaharwar, A.K., Iviglia, G., Zhang, H., Mukundan, S., Mihaila, S.M., *et al.* Highly elastomeric poly (glycerol sebacate)- *co*-poly (ethylene glycol) amphiphilic block copolymers. Biomaterials **34,** 3970. 2013.
13. Agrawal, C., and Ray, R.B. Biodegradable polymeric scaffolds for musculoskeletal tissue engineering. J Biomed Mater Res **55,** 141, 2001.
14. Zhang, H., Patel, A., Gaharwar, A.K., Mihaila, S.M., Iviglia, G.I., Mukundan, S., *et al.* Hyperbranched polyester hydrogels with controlled drug release and cell adhesion properties. Biomacromolecules **14,** 1299, 2013.
15. Lam, C.X.F., Hutmacher, D.W., Schantz, J.T., Woodruff, M.A., and Teoh, S.H. Evaluation of polycaprolactone scaffold degradation for 6 months *in vitro* and *in vivo*. J Biomed Mater Res Part A **90,** 906, 2008.

16. Pitt, C.G., Chasalow, F.I., Hibionada, Y.M., Klimas, D.M., and Schindler, A. Aliphatic polyesters. I. The degradation of poly(ε-caprolactone) *in vivo*. J Appl Polym Sci **26,** 3779, 1981.
17. Sant, S., Hwang, C.M., Lee, S.-H., and Khademhosseini, A. Hybrid PGS–PCL microfibrous scaffolds with improved mechanical and biological properties. J Tissue Eng Regen Med **5,** 283, 2011.
18. Liao, G., Jiang, S., Xu, X., and Ke, Y. Electrospun aligned PLLA/PCL/HA composite fibrous membranes and their *in vitro* degradation behaviors. Mater Lett **82,** 159, 2012.
19. Wutticharoenmongkol, P., Sanchavanakit, N., Pavasant, P., and Supaphol, P. Preparation and characterization of novel bone scaffolds based on electrospun polycaprolactone fibers filled with nanoparticles. Macromol Biosci **6,** 70, 2006.
20. Ganesh, N., Jayakumar, R., Koyakutty, M., Mony, U., and Nair, S.V. Embedded silica nanoparticles in poly (caprolactone) nanofibrous scaffolds enhanced osteogenic potential for bone tissue engineering. Tissue Eng Part A **18,** 1867, 2012.
21. Wu, C.-J., Gaharwar, A.K., Schexnailder, P.J., and Schmidt, G. Development of biomedical polymer-silicate nanocomposites: a materials science perspective. Materials **3,** 2986, 2010.
22. Bordes, P., Pollet, E., and Avérous, L. Nano-biocomposites: Biodegradable polyester/nanoclay systems. Prog Polym Sci **34,** 125, 2009.
23. Gaharwar, A.K., Schexnailder, P.J., Kaul, V., Akkus, O., Zakharov, D., Seifert, S., *et al.* Highly extensible bionanocomposite films with direction-dependent properties. Adv Funct Mater **20,** 429, 2010.
24. Gaharwar, A.K., Schexnailder, P.J., Dundigalla, A., White, J.D., Matos-Pérez, C.R., Cloud, J.L., *et al.* Highly extensible bio-nanocomposite fibers. Macromol Rapid Commun **32,** 50, 2011.
25. Liff, S.M., Kumar, N., and McKinley, G.H. High-performance elastomeric nanocomposites via solvent-exchange processing. Nat Mater **6,** 76, 2007.
26. Podsiadlo, P., Kaushik, A.K., Arruda, E.M., Waas, A.M., Shim, B.S., Xu, J., *et al.* Ultrastrong and stiff layered polymer nanocomposites. Science **318,** 80, 2007.
27. Bonderer, L.J., Studart, A.R., and Gauckler, L.J. Bioinspired design and assembly of platelet reinforced polymer films. Science **319,** 1069, 2008.
28. Priolo, M.A., Gamboa, D., Holder, K.M., and Grunlan, J.C. Super gas barrier of transparent polymer–clay multilayer ultrathin films. Nano Lett **10,** 4970, 2010.
29. Lin, L., Liu, M., Chen, L., Chen, P., Ma, J., Han, D., *et al.* Bio-inspired hierarchical macromolecule–nanoclay hydrogels for robust underwater superoleophobicity. Adv Mater **22,** 4826, 2010.
30. Li, Y.-C., Schulz, J., Mannen, S., Delhom, C., Condon, B., Chang, S., *et al.* Flame retardant behavior of polyelectrolyte–clay thin film assemblies on cotton fabric. ACS Nano **4,** 3325, 2010.
31. Wang, Q., Mynar, J.L., Yoshida, M., Lee, E., Lee, M., Okuro, K., *et al.* High-water-content mouldable hydrogels by mixing clay and a dendritic molecular binder. Nature **463,** 339, 2010.
32. Gaharwar, A.K., Mihaila, S.M., Swami, A., Patel, A., Sant, S., Reis, R.L., *et al.* Bioactive silicate nanoplatelets for osteogenic diffrentiation of human human mesenchymal stem cells. Adv Mater **24,** 3329, 2013.
33. Schexnailder, P.J., Gaharwar, A.K., Bartlett II, R.L., Seal, B.L., and Schmidt, G. Tuning cell adhesion by incorporation of charged silicate nanoparticles as cross-linkers to polyethylene oxide. Macromol Biosci **10,** 1416, 2010.
34. Gaharwar, A.K., Kishore, V., Rivera, C., Bullock, W., Wu, C.J., Akkus, O., *et al.* Physically crosslinked nanocomposites from silicate-crosslinked PEO: mechanical properties and osteogenic differentiation of human mesenchymal stem cells. Macromol Biosci **12,** 779. 2012.
35. Gaharwar, A.K., Schexnailder, P.J., and Schmidt, G. Nanocomposite polymer biomaterials for tissue repair of bone and cartilage: a material science perspective. Taylor and Francis Group, 2011.
36. Marras, S.I., Kladi, K.P., Tsivintzelis, I., Zuburtikudis, I., and Panayiotou, C. Biodegradable polymer nanocomposites: the role of nanoclays on the thermomechanical characteristics and the electrospun fibrous structure. Acta Biomater **4,** 756, 2008.
37. Nitya, G., Nair, G.T., Mony, U., Chennazhi, K.P., and Nair, S.V. *In vitro* evaluation of electrospun PCL/nanoclay composite scaffold for bone tissue engineering. J Mater Sci Mater Med **23,** 1749, 2012.
38. Gaharwar, A.K., Schexnailder, P., Kaul, V., Akkus, O., Zakharov, D., Seifert, S., *et al.* Highly Extensible bionanocomposite films with direction-dependent properties. Adv Funct Mater **20,** 429, 2010.
39. Gaharwar, A.K., Schexnailder, P.J., Kline, B.P., and Schmidt, G. Assessment of using Laponite® cross-linked poly(ethylene oxide) for controlled cell adhesion and mineralization. Acta Biomater **7,** 568, 2011.
40. Ambre, A.H., Katti, D.R., and Katti, K.S. Nanoclays mediate stem cell differentiation and mineralized ECM formation on biopolymer scaffolds. J Biomed Mater Res Part A **101A,** 2644, 2013.
41. Sant, S., Iyer, D., Gaharwar, A., Patel, A., and Khademhosseini, A. Effect of biodegradation and *de novo* matrix synthesis on the mechanical properties of VIC-seeded PGS-PCL scaffolds. Acta Biomater **9,** 5963, 2012.
42. Armentano, I., Del Gaudio, C., Bianco, A., Dottori, M., Nanni, F., Fortunati, E., *et al.* Processing and properties of poly (ε-caprolactone)/carbon nanofibre composite mats and films obtained by electrospinning and solvent casting. J Mater Sci **44,** 4789, 2009.
43. Guo, Q., Harrats, C., Groeninckx, G.l., and Koch, M. Miscibility, crystallization kinetics and real-time small-angle X-ray scattering investigation of the semicrystalline morphology in thermosetting polymer blends of epoxy resin and poly (ethylene oxide). Polymer **42,** 4127, 2001.
44. Kokubo, T., and Takadama, H. How useful is SBF in predicting *in vivo* bone bioactivity? Biomaterials **27,** 2907, 2006.
45. Oyane, A., Kim, H.-M., Furuya, T., Kokubo, T., Miyazaki, T., and Nakamura, T. Preparation and assessment of revised simulated body fluids. J Biomed Mater Res Part A **65A,** 188, 2003.
46. Thomas, V., Jagani, S., Johnson, K., Jose, M.V., Dean, D.R., Vohra, Y.K., *et al.* Electrospun bioactive nanocomposite scaffolds of polycaprolactone and nanohydroxyapatite for bone tissue engineering. J Nanosci Nanotechnol **6,** 487, 2006.
47. Thomas, V., Dean, D.R., Jose, M.V., Mathew, B., Chowdhury, S., and Vohra, Y.K. Nanostructured biocomposite scaffolds based on collagen coelectrospun with nanohydroxyapatite. Biomacromolecules **8,** 631, 2007.

48. Li, C., Vepari, C., Jin, H.-J., Kim, H.J., and Kaplan, D.L. Electrospun silk-BMP-2 scaffolds for bone tissue engineering. Biomaterials **27,** 3115, 2006.
49. Lam, C.X.F., Savalani, M.M., Teoh, S.-H., and Hutmacher, D.W. Dynamics of *in vitro* polymer degradation of polycaprolactone-based scaffolds: accelerated versus simulated physiological conditions. Biomed Mater **3,** 034108, 2008.
50. Dong, Y., Liao, S., Ngiam, M., Chan, C.K., and Ramakrishna, S. Degradation behaviors of electrospun resorbable polyester nanofibers. Tissue Eng Part B Rev **15,** 333, 2009.
51. Persenaire, O., Alexandre, M., Degée, P., and Dubois, P. Mechanisms and kinetics of thermal degradation of poly(ε-caprolactone). Biomacromolecules **2,** 288, 2001.
52. Engler, A.J., Sen, S., Sweeney, H.L., and Discher, D.E. Matrix elasticity directs stem cell lineage specification. Cell **126,** 677, 2006.
53. Kokubo, T. Bioactive glass ceramics: properties and applications. Biomaterials **12,** 155, 1991.
54. Oyane, A., Uchida, M., Choong, C., Triffitt, J., Jones, J., and Ito, A. Simple surface modification of poly (ε-caprolactone) for apatite deposition from simulated body fluid. Biomaterials **26,** 2407, 2005.
55. Nair, L.S., and Laurencin, C.T. Biodegradable polymers as biomaterials. Prog Polym Sci **32,** 762, 2007.
56. Pittenger, M.F., Mackay, A.M., Beck, S.C., Jaiswal, R.K., Douglas, R., Mosca, J.D., *et al.* Multilineage potential of adult human mesenchymal stem cells. Science **284,** 143, 1999.
57. Moore, K.A., and Lemischka, I.R. Stem cells and their niches. Science **311,** 1880, 2006.
58. Lutolf, M., and Hubbell, J. Synthetic biomaterials as instructive extracellular microenvironments for morphogenesis in tissue engineering. Nat Biotechnol **23,** 47, 2005.
59. Moroni, L., Licht, R., de Boer, J., de Wijn, J.R., and van Blitterswijk, C.A. Fiber diameter and texture of electrospun PEOT/PBT scaffolds influence human mesenchymal stem cell proliferation and morphology, and the release of incorporated compounds. Biomaterials **27,** 4911, 2006.
60. Gaharwar, A.K., Dammu, S.A., Canter, J.M., Wu, C.-J., and Schmidt, G. Highly extensible, tough, and elastomeric nanocomposite hydrogels from poly(ethylene glycol) and hydroxyapatite nanoparticles. Biomacromolecules **12,** 1641, 2011.
61. Gaharwar, A.K., Rivera, C., Wu, C.-J., Chan, B.K., and Schmidt, G. Photocrosslinked nanocomposite hydrogels from PEG and silica nanospheres: Structural, mechanical and cell adhesion characteristics. Mater Sci Eng C **33,** 1800, 2013.
62. Binulal, N., Deepthy, M., Selvamurugan, N., Shalumon, K., Suja, S., Mony, U., *et al.* Role of nanofibrous poly (caprolactone) scaffolds in human mesenchymal stem cell attachment and spreading for *in vitro* bone tissue engineering—response to osteogenic regulators. Tissue Eng Part A **16,** 393, 2010.

Address correspondence to:
Ali Khademhosseini, PhD
Harvard-MIT Division of Health Sciences and Technology
Massachusetts Institute of Technology
65 Landsdowne St., #252
Cambridge, MA 02139

E-mail: alik@rics.bwh.harvard.edu

Received: May 14, 2013
Accepted: December 12, 2013
Online Publication Date: May 15, 2014